Theoretical Study of Ultrafast Heterogeneous Electron Transfer Reactions at Dye−Semiconductor Interfaces: Coumarin 343 at Titanium Oxide†

Ivan Kondov and Michael Thoss*

Department of Chemistry, Technical University of Munich, D-85748 Garching, Germany

Haobin Wang*

Department of Chemistry and Biochemistry, MSC 3C, New Mexico State University, Las Cruces, New Mexico 88003

Received: July 27, 2005; In Final Form: September 24, 2005

A theoretical study of photoinduced heterogeneous electron transfer in the dye−semiconductor system coumarin 343−TiO_2 is presented. The study is based on a generic model for heterogeneous electron transfer reactions, which takes into account the coupling of the electronic states to the nuclear degrees of freedom of coumarin 343 as well as to the surrounding solvent. The quantum dynamics of the electron injection process is simulated employing the recently proposed multilayer formulation of the multiconfiguration time-dependent Hartree method. The results reveal an ultrafast injection dynamics of the electron from the photoexcited donor state into the conduction band of the semiconductor. Furthermore, the mutual influence of electronic injection dynamics and nuclear motion is analyzed in some detail. The analysis shows that—depending on the time scale of nuclear motion—electronic vibrational coupling can result in electron transfer driven by coherent vibrational motion or vibrational motion induced by ultrafast electron transfer.

1. Introduction

Photoinduced electron transfer (ET) reactions at dye−semiconductor interfaces represent an interesting class of ET processes. In particular, the process of electron injection from an electronically excited state of a dye molecule to a semiconductor substrate has been investigated in great detail experimentally in recent years.[1−15] This process represents a key step for photonic energy conversion in nanocrystalline solar cells.[2,5,7,16,17] Employing femtosecond spectroscopy techniques, it has been demonstrated that electron injection processes often take place on an ultrafast time scale. Electron injection as fast as 6 fs has been reported for alizarin adsorbed on TiO_2 nanoparticles.[12] For other sensitizing chromophores, e.g., coumarin 343[3,5,11,18,19] or perylene,[6,20] injection times on the order of tens to hundreds of femtoseconds have been found. Studies of dye molecules with electron injection time scales on the order of a few tens to a few hundred femtoseconds also indicate that the coupling to the vibrational modes of the chromophore may have a significant impact on the injection dynamics.[6,20,21] In particular, the influence of coherent vibrational motion on the injection dynamics has been observed in studies of perylene adsorbed on TiO_2 nanoparticles.[6,20] Other important effects that have been investigated experimentally are the influence of surface trap states[22,23] as well as bridging groups[24] on the kinetics of the electron injection process.

The theoretical modeling of ET at dye−semiconductor interfaces requires in principle a simulation of the electron injection dynamics. While for very fast injection processes ($\lesssim$10 fs) the dynamical influence of the nuclear degrees of freedom on the electron injection process is presumably of minor importance and one may consider the purely electronic injection dynamics,[25] for ET reactions on the order of a few tens to a few hundred femtoseconds, the coupling to the nuclear degrees of freedom has to be included in the dynamical simulation. Because a full quantum dynamical simulation of the ET dynamics including the coupling to the nuclear degrees of freedom and employing an adequate electronic structure theory is currently not feasible, different approximate strategies have been applied. One possibility is to use a first principle electronic structure method to describe the dye−semiconductor system but employ an approximate dynamical method. An example is ab initio molecular dynamics, where the dynamics of the nuclear degrees of freedom is described classically.[26−31] On the other hand, one can use physically motivated models to study ET processes at interfaces, such as the Anderson−Newns model,[32] which allows an accurate description of the dynamics. Along this line, several workers have studied the electron injection dynamics based on models of reduced dimensionality, taking into account typically a single reaction mode.[15,33−39] Dissipative effects, such as vibrational relaxation of the reaction mode, have been considered (for weak coupling) within Redfield theory.[36] In a recent model study, we have investigated in detail the influence of multidimensional coherent and dissipative vibrational motion on the electron injection dynamics[40] employing the self-consistent hybrid approach[41,42] in combination with the multilayer multiconfiguration time-dependent Hartree method.[43] These methods allow an accurate quantum dynamical description of the ET process beyond the limitations of perturbation theory.

To apply such models to experimentally relevant systems, various model parameters such as the energies and couplings of the relevant electronic states, the important vibrational modes of the chromophore, as well as the electronic vibrational couplings need to be determined. As a first step to this end, we

† Part of the special issue "William Hase Festschrift".

* To whom correspondence should be addressed. (M.T.) E-mail: michael.thoss@ch.tum.de. (H.W.) E-mail: whb@intrepid.nmsu.edu.

10.1021/jp054162z CCC: $33.50
Published on Web 11/04/2005

have recently carried out electronic structure studies of small complexes of titanium with three chromophores: catechol, alizarin, and coumarin 343.[44] In qualitative agreement with experimental results and other electronic structure calculations,[30] this study showed that the character of the photoexcited states is qualitatively different in the three chromophores: While in catechol a number of low-lying charge transfer states appear upon formation of the catechol−TiO_2 complex, the lowest excited states of the complex of coumarin 343 as well as of one of the alizarin complexes are predominantly localized at the chromophore and only exhibit redshifts with respect to the corresponding isolated chromophores. Furthermore, this study also revealed that in all three chromophores, the electronic vibrational coupling is distributed over a relatively large number of vibrational modes of the respective chromophore.

In this paper, we will consider the electronic injection dynamics of the dye−semiconductor system coumarin 343−TiO_2. The ET dynamics in this system has been studied experimentally by a number of groups in recent years.[3,5,11,18,19] Employing different techniques, injection times in the range of 20−200 fs have been found. These results in combination with the localized character of the photoexcited state in this system suggest that the coumarin 343−TiO_2 system is particularly well-suited to study the electron injection dynamics as well as the influence of the nuclear degrees of freedom on the ET process. Besides the fundamental interest in the electron injection mechanism, coumarin derivatives have also been investigated as alternative organic photosensitizers in nanocrystalline solar cells.[45]

The remainder of this paper is organized as follows: In section 2, we introduce the ET model for the coumarin 343−TiO_2 system. Following a brief description of the different observables used to characterize the ET reaction, we give a short outline of the multilayer multiconfiguration time-dependent Hartree method, which is used to describe the quantum dynamics. The results of the simulations are discussed in section 3. Besides the electronic injection dynamics, we shall consider the absorption spectrum of the dye−semiconductor system and the nuclear dynamics associated with the ET reaction. In particular, we will discuss the mutual influence of electron injection dynamics and nuclear motion based on results for the wave packet dynamics of selected vibrational modes of coumarin 343. Section 4 concludes with a summary.

2. Theory

A. Model of the ET Reaction. To study the dynamics of ultrafast photoinduced electron injection from the electronically excited state of the chromophore coumarin 343 (in the following abbreviated as C343) into the conduction band of the semiconductor (TiO_2) substrate, we consider a model based on an Anderson−Newns type Hamiltonian.[32,40,46−48] Within this model, the Hamiltonian is represented in a basis of the following diabatic (charge localized) electronic states, which are relevant for the photoreaction: the electronic ground state of the overall system $|\phi_g\rangle$, the donor state of the ET process $|\phi_d\rangle$ (which, in the limit of vanishing coupling between chromophore and semiconductor substrate, corresponds to the product of the first electronically excited state of C343 and an empty conduction band of the semiconductor), and the (quasi)continuum of acceptor states of the ET reaction $|\phi_k\rangle$ (corresponding in the zero coupling limit to the product of the cationic state of C343 and an electron with energy ϵ_k in the conduction band of the semiconductor substrate). Thus, the Hamiltonian reads

$$H_s = T + |\phi_g\rangle V_g \langle\phi_g| + |\phi_d\rangle V_d \langle\phi_d| + \sum_k |\phi_k\rangle (\epsilon_k + V_a) \langle\phi_k| + \sum_k (|\phi_d\rangle V_{dk} \langle\phi_k| + |\phi_k\rangle V_{kd} \langle\phi_d|) \quad (1)$$

with the kinetic energy of the nuclei (we use mass-scaled coordinates and atomic units where $\hbar = 1$ throughout the paper)

$$T = \frac{1}{2}\sum_l P_l^2 \quad (2)$$

and the diabatic potential matrix $V_{ij}(\mathbf{Q})$, which depends on the nuclear coordinates $\mathbf{Q}$. The nuclear degrees of freedom include in principle both the phonons of the semiconductor substrate and the intramolecular vibrations of the chromophore. In this paper, we only consider the intramolecular vibrations, which are expected to have a larger influence on the electron injection process due to the ultrafast time scale of the ET reaction.

To describe the vibrational degrees of freedom of the chromophore, we employ the harmonic approximation for the potential energy in the electronic ground state of C343

$$V_g(Q) = \epsilon_g + \frac{1}{2}\sum_l \Omega_l^2 Q_l^2 \quad (3)$$

where Q_l denotes the l-th normal mode in the electronic ground state of C343 (with frequency Ω_l) and ϵ_g is the ground state equilibrium energy. To account for electronic vibrational coupling, we expand the diabatic potential energy surfaces of the other electronic states about the equilibrium geometry of the electronic ground state

$$V_d(Q) = \epsilon_d + \sum_l \kappa_l^d Q_l + \sum_{lk} \gamma_{lk}^d Q_l Q_k \quad (4a)$$

$$V_a(Q) = \epsilon_a + \sum_l \kappa_l^a Q_l + \sum_{lk} \gamma_{lk}^a Q_l Q_k \quad (4b)$$

Here, ϵ_d and ϵ_a denote the energy of the donor and acceptor state (at the equilibrium geometry of the ground state), respectively. Because only the sum of the energies ϵ_k and ϵ_a enter the Hamiltonian H_s (cf. eqs 1 and 4b), we will for notational simplicity in the following denote this sum by ϵ_k.

Within the Anderson−Newns model (and for vanishing coupling between chromophore and semiconductor substrate), the potential energy surfaces of the donor and acceptor state, $V_d(\mathbf{Q})$ and $V_a(\mathbf{Q})$, are given by the potential energy functions of the excited state of neutral C343 and the ground state of the cation of C343, respectively. In the simplest approximation, only the linear and diagonal quadratic terms in the expansion (eq 4) are taken into account. Furthermore, the frequencies are approximated by their ground state state values, and Dushinski rotation[49] of the normal modes is neglected. In this way, we obtain

$$V_d(Q) = \epsilon_d + \sum_l \kappa_l^d Q_l + \frac{1}{2}\sum_l \Omega_l^2 Q_l^2 \quad (5a)$$

$$V_a(Q) = \epsilon_a + \sum_l \kappa_l^a Q_l + \frac{1}{2}\sum_l \Omega_l^2 Q_l^2 \quad (5b)$$

The thus obtained potential energy surfaces of the ET model are schematically illustrated in Figure 1.

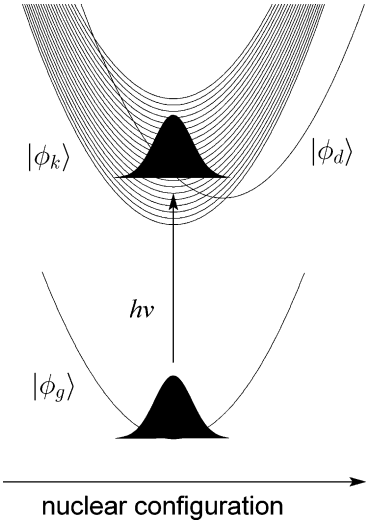

Figure 1. Schematic illustration of the potential energy surfaces of the donor and acceptor states along one of the nuclear coordinates. In addition, the ground state, from which photoexcitation to the donor state takes place, is shown.

The electronic vibrational coupling constants κ_l^{d}, κ_l^{a} are related to reorganization energies via

$$\lambda_l^{\mathrm{d}} = \frac{(\kappa_l^{\mathrm{d}})^2}{2\Omega_l^2} \tag{6a}$$

$$\lambda_l^{\mathrm{a}} = \frac{(\kappa_l^{\mathrm{a}})^2}{2\Omega_l^2} \tag{6b}$$

which are associated with transitions from the electronic ground state to the excited state and the cation of C343, respectively. The reorganization energy for the ET process, which corresponds to a transition from the excited state of the chromophore to the cation, is given by

$$\lambda_l^{\mathrm{ET}} = \frac{(\kappa_l^{\mathrm{d}} - \kappa_l^{\mathrm{a}})^2}{2\Omega_l^2} \tag{7}$$

for the l-th intramolecular mode and the total reorganization energy of the intramolecular modes by the sum $\lambda_{\mathrm{s}}^{\mathrm{ET}} = \sum_l \lambda_l^{\mathrm{ET}}$.

The normal modes Q_l, their frequencies Ω_l, and the electronic vibrational coupling constants κ_l^{d}, κ_l^{a} have been determined by electronic structure calculations for the isolated chromophore C343.[44] As described in detail in ref 44, this includes geometry optimization of the electronic ground state of C343, determination of the corresponding normal modes, and the calculation of the energy gradients along the normal modes in the first electronically excited state of C343 (which, in combination with an empty conduction band, describes the donor state of the ET reaction within the Anderson−Newns model) and the ground state of the cation of C343 (which in combination with a single electron in the conduction band of the semiconductor models the acceptor states). All electronic structure calculations have been performed with the program package TURBOMOLE[50] employing density functional theory with the B-P functional and a triple-ζ basis set [TZV(P)]. A comparison of results based on different functionals as well as calculations employing the HF and CIS method has been given in ref 44. The calculated frequencies and reorganization energies of the intramolecular modes are depicted in Figures 2 and 3. All parameters are given in Table 1. The overall reorganization energies obtained are $\lambda_{\mathrm{s}}^{\mathrm{d}} = 1010\ \mathrm{cm}^{-1}$, $\lambda_{\mathrm{s}}^{\mathrm{a}} = 976\ \mathrm{cm}^{-1}$, and $\lambda_{\mathrm{s}}^{\mathrm{ET}} = 2444\ \mathrm{cm}^{-1}$ for the donor state, the acceptor state, and the ET transition, respectively.

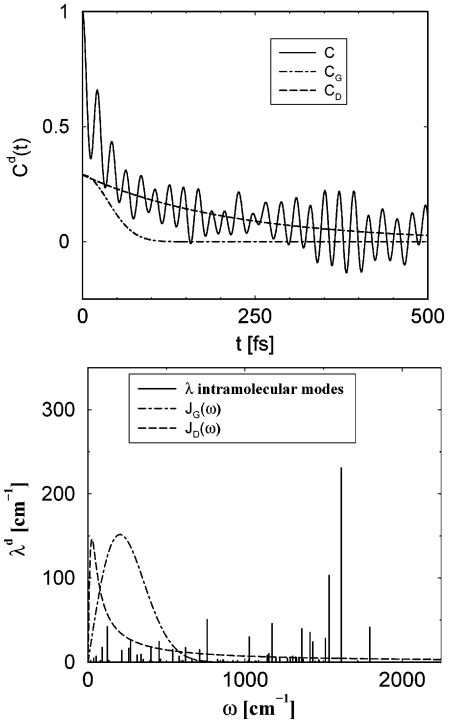

Figure 2. Properties of the nuclear degrees of freedom of the ET model associated with the transition from the ground to the electronically excited state of C343. Upper panel: total (inner + outer sphere) normalized energy gap correlation function $C^{\mathrm{d}}(t)/C^{\mathrm{d}}(0)$ (full line) as well as separate contributions of the Gaussian (dashed−dotted line) and the Debye (dashed line) part of the spectral density. Lower panel: Gaussian (dashed−dotted line) and Debye (dashed line) part of the spectral density of the solvent environment as well as reorganization energies of the intramolecular modes of C343. The spectral densities have been scaled for better illustration.

The electronic coupling between the donor state and the continuum of acceptor states is determined by the coupling matrix elements V_{dk}, which are assumed to be approximately independent of the nuclear degrees of freedom. The coupling matrix elements V_{dk} and the distribution of energies ϵ_k of the conduction band of the semiconductor can be specified by the energy-dependent decay width of the donor state

$$\Gamma(E) = 2\pi \sum_k |V_{\mathrm{dk}}|^2\, \delta(E - \epsilon_k) \tag{8}$$

which describes the coupling-weighted density of states of the semiconductor substrate.

In principle, the energy-dependent decay width $\Gamma(E)$ can be determined employing electronic structure theory calculations.[51] In the studies below, we have adopted a parametrization based on a tight-binding model, which has been developed recently by Petersson et al.[52] to study the electron injection rate from an excited state of a dye molecule to a semiconductor substrate. Within this tight-binding model, the energy-dependent decay width of the donor state is given by

$$\Gamma(E) = \begin{cases} \dfrac{2v_0^2(E - E_0)}{v^2} \sqrt{1 - \left[\dfrac{(E - E_0)^2 - \epsilon^2 - 2v^2}{2v^2}\right]^2} & \text{if } E_0 + \epsilon \le E \le E_0 + \sqrt{4v^2 + \epsilon^2} \\ 0 & \text{otherwise} \end{cases} \tag{9}$$

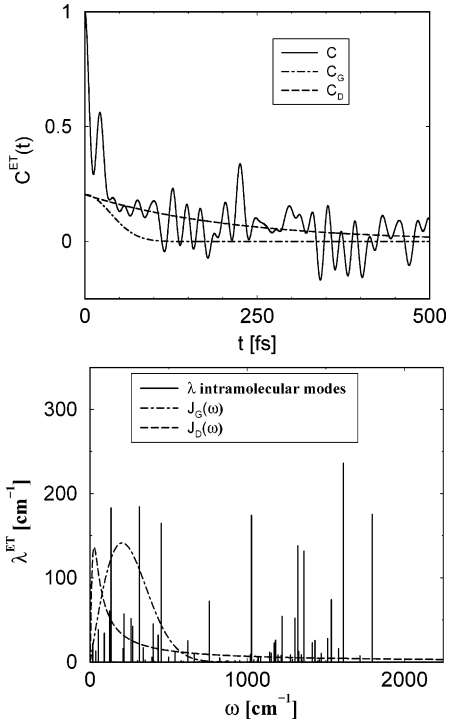

Figure 3. Properties of the nuclear degrees of freedom of the ET model associated with the ET transition, i.e., the transition from the electronically excited state of neutral C343 to the electronic ground state of the cation of C343. Upper panel: total (inner + outer sphere) normalized energy gap correlation function $C^{ET}(t)/C^{ET}(0)$ (full line) as well as separate contributions of the Gaussian (dashed−dotted line) and the Debye (dashed line) part of the spectral density. Lower panel: Gaussian (dashed−dotted line) and Debye (dashed line) part of the spectral density of the solvent environment as well as reorganization energies of the intramolecular modes of C343. The spectral densities have been scaled for better illustration.

TABLE 1: Calculated Ground State Harmonic Frequencies and Electronic Vibrational Coupling Constants in the Excited State and in the Cation of C343 (All Data in cm^{-1})[a]

mode	Ω_j	$\kappa_j^d/\sqrt{\Omega_j}$	$\kappa_j^a/\sqrt{\Omega_j}$	mode	Ω_j	$\kappa_j^d/\sqrt{\Omega_j}$	$\kappa_j^a/\sqrt{\Omega_j}$
1	17	−8	19	30	621	147	−30
2	36	−19	12	31	661	77	195
3	53	28	−36	34	710	−146	−156
4	78	18	18	35	758	277	−53
5	90	56	−22	48	1020	−70	−204
6	122	102	−20	49	1026	248	−350
7	133	−23	198	55	1151	152	307
9	209	−17	−98	56	1172	328	98
10	215	−78	79	57	1180	18	265
11	260	93	−70	61	1221	120	−244
12	271	118	−34	65	1303	137	−231
14	312	73	−266	66	1321	127	−477
15	337	−80	27	72	1360	−330	269
17	394	−36	30	74	1413	316	61
18	401	−117	73	75	1431	−264	8
20	433	−15	151	82	1511	−292	−1
21	452	149	−236	83	1534	563	86
25	539	127	18	85	1612	−863	10
27	580	−91	−131	87	1795	387	−407

[a] Only data selected for the dynamical simulations are shown.

where E_0 is the mean energy value of the conduction and valence band, $\pm\epsilon$ describe the site energies for the different atoms in the metal oxide semiconductor, v denotes the nearest-neighbor coupling matrix element, and v_0 specifies the coupling between the semiconductor and the chromophore (for details, see ref 52). In the numerical calculations considered below, we have adopted the parameters of Petersson et al. ($E_0 = -1.6$ eV, $v = 2$ eV, and $\epsilon = 1.6$ eV), which were determined to resemble the lower 3d group of the TiO_2 conduction band. For notational simplicity, the parameter E_0, which defines the absolute energy scale of the model, was changed as compared to ref 52 such that the bottom of the conduction band (given by $E_0 + \epsilon$) is at zero energy. The overall strength of the electronic coupling v_0 as well as the energy of the donor state, ϵ_d, relative to the conduction band edge of the titanium oxide semiconductor have been determined by comparison of the absorption spectrum predicted by the model with the experimental absorption spectra (see section 3).

In most experiments on electron injection from C343 to semiconductor substrates, a colloidal solution of dye-sensitized nanoparticles was employed.[3,5,11,19] To account for the influence of the surrounding solvent on the ET dynamics in our simulations, we employ a standard (outer sphere) linear response model[53−55] where the Hamiltonian of the dye−semiconductor system is coupled linearly to a bath of harmonic oscillators. Thus, the Hamiltonian of the overall system reads

$$H = H_s + H_b + H_{sb} \tag{10}$$

with H_s given by eq 1 and

$$H_b = \frac{1}{2}\sum_j (p_j^2 + \omega_j^2 x_j^2), \tag{11a}$$

$$H_{sb} = |\phi_d\rangle \sum_j c_j^d x_j \langle\phi_d| + \sum_k |\phi_k\rangle \sum_j c_j^a x_j \langle\phi_k| \tag{11b}$$

The parameters of the solvent part of the Hamiltonian are characterized by the spectral densities

$$J_b^d(\omega) = \frac{\pi}{2}\sum_j \frac{(c_j^d)^2}{\omega_j}\delta(\omega - \omega_j) \tag{12a}$$

$$J_b^a(\omega) = \frac{\pi}{2}\sum_j \frac{(c_j^a)^2}{\omega_j}\delta(\omega - \omega_j) \tag{12b}$$

The spectral densities describe the response of the solvent polarization to the change of the charge distribution of the solute associated with electronic transitions from the ground electronic state to the excited state of the chromophore and to the cation, respectively. In principle, the spectral densities can be different for the two electronic transitions. Here, we use for simplicity a modeling where the response of the solvent for both transitions is described by a coupling to the same bath, which differs only in the overall coupling strength, i.e., $c_j^a = \alpha c_j^d$ (accordingly, in the following, the superscript for the coupling constants will be omitted, i.e., $c_j \equiv c_j^d$). It is noted that this approximation is only invoked for the solvent bath modes but not for the intramolecular modes. This description is in accordance with simple dielectric continuum theories of relaxation in polar solvents,[55−57] which result in a spectral density of the form

$$J_b(\omega) \sim \frac{\lambda}{c_p}\frac{\mathrm{Im}[\epsilon(\omega)]}{|\epsilon(\omega)|^2} \tag{13}$$

where $\epsilon(\omega)$ is the dielectric function of the solvent and the Pekar factor $c_p = \epsilon_\infty^{-1} - \epsilon_0^{-1}$ involves the static (ϵ_0) and high-frequency (ϵ_∞) limit of the dielectric function. In this description, only the reorganization energy λ depends on the charge distribution and thus on the electronic state of the solute. As a

result of this assumption, we have

$$J_b^a(\omega) = \alpha^2 J_b^d(\omega) = \alpha^2 \frac{\pi}{2} \sum_j \frac{c_j^2}{\omega_j} \delta(\omega - \omega_j) \tag{14}$$

The bath reorganization energies associated with the transitions from the electronic ground to the excited state and to the cation of the chromophore are given by

$$\lambda_b^d = \sum_j \frac{(c_j^d)^2}{2\omega_j^2} \equiv \sum_j \frac{c_j^2}{2\omega_j^2} \tag{15a}$$

$$\lambda_b^a = \sum_j \frac{(c_j^a)^2}{2\omega_j^2} = \alpha^2 \sum_j \frac{c_j^2}{2\omega_j^2} \tag{15b}$$

The reorganization energy for the ET process, which corresponds to a transition from the electronically excited state to the cation of the chromophore, on the other hand, is given by

$$\lambda_b^{ET} = \sum_j \frac{(c_j^d - c_j^a)^2}{2\omega_j^2} = (1-\alpha)^2 \sum_j \frac{c_j^2}{2\omega_j^2} \tag{16}$$

It is noted that in the current model the three different reorganization energies of the bath fulfill the relation[58,59] $\lambda_b^a = (\sqrt{\lambda_b^d} - \sqrt{\lambda_b^{ET}})^2$.

The spectral densities introduced above are related to the (classical) energy gap correlation functions

$$C_b^d(t) \sim \frac{1}{\pi} \int_0^\infty d\omega \frac{J^d(\omega)}{\omega} \cos(\omega t) \tag{17a}$$

$$C_b^a(t) \sim \frac{1}{\pi} \int_0^\infty d\omega \frac{J^a(\omega)}{\omega} \cos(\omega t) \tag{17b}$$

which describe the influence of the solvent on the energy gap between the ground state and the donor state and the ground state and the acceptor states, respectively.

For some systems, $C_b(t)$ can be obtained from classical molecular dynamics simulations.[60,61] Here, we take a more phenomenological approach based on recent experimental and theoretical observations that the solvation dynamics in many polar solvents involve typically (at least) two important time scales:[62,63] an ultrafast inertial decay of Gaussian character and a slower diffusive decay of exponential form. Accordingly, we model the bath by a bimodal spectral density

$$J_b(\omega) = J_G(\omega) + J_D(\omega) \tag{18}$$

with a Gaussian part accounting for the ultrafast inertial decay

$$J_G(\omega) = \sqrt{\pi} \frac{\lambda_G \omega}{\omega_G} e^{-[\omega/(2\omega_G)]^2} \tag{19a}$$

and a Debye part describing the slower diffusive decay

$$J_D(\omega) = 2\lambda_D \frac{\omega \omega_D}{\omega^2 + \omega_D^2} \tag{19b}$$

The corresponding classical energy gap correlation function $C_b(t)$ is then given by

$$C_b(t) \sim \lambda_G e^{-(t/\tau_G)^2} + \lambda_D e^{-t/\tau_D} \tag{20}$$

where we have introduced the solvent relaxation times $\tau_G = 1/\omega_G$ and $\tau_D = 1/\omega_D$. The coupling strengths of the two parts of the spectral density are specified by the corresponding reorganization energies λ_G and λ_D, respectively.

Both the reorganization energies and the relaxation times depend on the specific solvent to be considered. Experiments on electron injection of C343-sensitized titanium nanoparticles have been performed in different solvents including methanol, acetone, and water.[3,5,11,19] Jimenez et al. have analyzed in detail the energy gap correlation function (associated with the transition from the electronic ground state to the excited state) for C343 in water.[62] They have shown that the energy gap correlation function can be fitted to a sum of a Gaussian function (which accounts for ≈50% of the overall reorganization energy), describing the fast inertial decay, and two Debye functions, modeling the slower diffusive decay. We have chosen the parameters of our model based on the analysis of Jimenez et al. as $\omega_G = 144.54\ cm^{-1}$ and $\omega_D = 25\ cm^{-1}$ corresponding to relaxation time scales of $\tau_G = 36.7$ fs and $\tau_D = 212.3$ fs. (Note that the two Gaussian functions in the analysis of Jimenez et al. have been contracted to a single function.)

The overall reorganization energy of the bath has been determined by fitting the width of the absorption spectrum of the C343 model (without coupling to the semiconductor substrate) to experimental results of Huber et al.[11,64] (see section 3). The thus obtained value of $\lambda_b^d = 1400\ cm^{-1}$ gives together with the reorganization energy of the intramolecular modes ($\lambda_s^d = 1010\ cm^{-1}$) an overall reorganization energy of $\lambda^d = 2510\ cm^{-1}$. This value is somewhat higher than the results of molecular dynamics simulations and estimates from time-dependent Stokes shift measurements by Maroncelli, Fleming, and co-workers.[62] Guided by the experimental results of Jimenez et al., the overall reorganization energy of the bath has been divided equally between the Gaussian and the Debye component of the spectral density resulting in $\lambda_D^d = \lambda_G^d = 700\ cm^{-1}$. The remaining bath parameter α is in our model determined by the (outer sphere) bath reorganization energy for the ET process λ_b^{ET} via the relation $\alpha = 1 - \sqrt{\lambda_b^{ET}/\lambda_b^d}$. Choosing λ_b^{ET} according to the electrostatic estimate for heterogeneous ET reactions[1] $\lambda_b^{ET} = 1693.7\ cm^{-1}$ results in a value $\alpha = -0.1$, which is used in the simulations.

To illustrate the different time scales of the nuclear degrees of freedom, it is instructive to consider the total (inner sphere + outer sphere) normalized energy gap correlation function

$$\frac{C(t)}{C(0)} = \frac{\int_0^\infty d\omega \frac{J(\omega)}{\omega} \cos(\omega t)}{\int_0^\infty d\omega \frac{J(\omega)}{\omega}} \tag{21}$$

which is given as the Fourier transform of the overall spectral density

$$J(\omega) = \frac{\pi}{2} \sum_l \frac{c_l^2}{\Omega_l} \delta(\omega - \Omega_l) + J_b(\omega) \tag{22}$$

Insertion of eqs 18 and 19 gives

$$\frac{C(t)}{C(0)} = \lambda^{-1}[\lambda_G e^{-(\omega_G t)^2} + \lambda_D e^{-\omega_D t} + \sum_l \lambda_l \cos(\Omega_l t)] \tag{23}$$

where $\lambda = \lambda_G + \lambda_D + \sum_l \lambda_l$ is the total reorganization energy. Figure 2 (upper panel) depicts the energy gap correlation function, $C^d(t)$, corresponding to the transition from the electronic ground state to the excited state of C343 together with separate contributions from the Gaussian and the Debye part of the bath spectral density. The corresponding spectral density of the bath as well as the reorganization energies of the intramolecular modes are illustrated in Figure 2 (lower panel). The respective quantities for the ET transition, i.e., the transition from the electronically excited state of neutral C343 to the ground state of the cation of C343, are shown in Figure 3. It is seen that for both transitions the electronic vibrational coupling is distributed over a relatively large number of intramolecular modes of C343. In the dynamical calculations presented below, 38 of the normal modes of C343 have been explicitly taken into account. These modes were selected according to their electronic vibrational coupling strength in the following way: All modes Q_l for which at least one of the dimensionless coupling parameters $\sqrt{\lambda_l^d/\Omega_l}$, $\sqrt{\lambda_l^a/\Omega_l}$, and $\sqrt{\lambda_l^{ET}/\Omega_l}$ is larger than a certain threshold (for the present calculation the threshold was chosen as 0.12) were included in the dynamical calculation. Test calculations with a larger number of intramolecular modes revealed no difference for the injection dynamics.

B. Observables of Interest. Several observables are of interest to study heterogeneous ET reactions at dye−semiconductor interfaces. The ET dynamics is most directly reflected by the time-dependent population of the donor state

$$P_d(t) = \frac{1}{\mathrm{tr}[e^{-\beta H_{Ng}}]}\mathrm{tr}[e^{-\beta H_{Ng}} |\phi_d\rangle \langle\phi_d| e^{iHt} |\phi_d\rangle \langle\phi_d| e^{-iHt}] \quad (24)$$

Here, we have assumed that the system is initially prepared by an ultrafast laser pulse in the donor state $|\phi_d\rangle$. The initial state of the nuclear degrees of freedom is specified by the Boltzmann operator $e^{-\beta H_{Ng}}$ of the nuclear Hamiltonian in the electronic ground state

$$H_{Ng} = \frac{1}{2}\sum_l (P_l^2 + \Omega_l^2 Q_l^2) + \frac{1}{2}\sum_j (p_j^2 + \omega_j^2 x_j^2) \quad (25)$$

To facilitate the interpretation of the ET dynamics, we shall also consider the associated vibrational dynamics of the intramolecular modes of C343. The vibrational dynamics of the l-th vibrational mode is described by the reduced density in the respective electronic state, which for the electronic donor state is given by

$$\rho_d(X_l, t) = \frac{1}{\mathrm{tr}[e^{-\beta H_{Ng}}]}\mathrm{tr}[e^{-\beta H_{Ng}} |\phi_d\rangle \langle\phi_d| e^{iHt} |\phi_d\rangle |X_l\rangle \langle X_l| \langle\phi_d| e^{-iHt}] \quad (26)$$

Here, $|X_l\rangle$ denotes the usual position eigenstate of the respective mode.

Finally, we will study the absorption spectrum of the chromophore C343 in solution as well as of the C343−semiconductor complex. The absorption spectrum is given by the Fourier transform of the dipole correlation function

$$I(\omega) \sim \frac{\omega}{2\pi}\int_{-\infty}^{\infty} \mathrm{d}t\, e^{i\omega t} C_{\mu\mu}(t) \quad (27a)$$

$$C_{\mu\mu}(t) = \frac{1}{Q}\mathrm{tr}\{e^{-\beta H}[\mu(t),\mu]\} \quad (27b)$$

with

$$\mu(t) \equiv e^{iHt}\mu\, e^{-iHt},\ Q = \mathrm{tr}[e^{-\beta H}] \quad (27c)$$

and

$$\mu = |\phi_d\rangle \mu_0 \langle\phi_g| + |\phi_g\rangle \mu_0 \langle\phi_d| \quad (27d)$$

Here, μ denotes the dipole operator. In eq 27d, we have assumed that the dipole operator is only weakly dependent on the nuclear coordinates (Condon approximation), and furthermore, direct excitations from the ground state of the chromophore to the conduction band of the semiconductor (which would not contribute directly to the electron injection dynamics) have been neglected. In the system considered in this paper, there is a relatively large energy difference between the ground and the photoexcited donor state. Therefore, we can invoke the approximation

$$e^{-\beta H} \simeq e^{-\beta H_{Ng}} |\phi_g\rangle \langle\phi_g|,\ Q \simeq \mathrm{tr}[e^{-\beta H_{Ng}}] \quad (28)$$

which corresponds to a factorized initial state. The extension of the method to simulate quantum dynamics in the condensed phase for a correlated initial state is described in ref 65.

C. Dynamical Approach: Multilayer Formulation of the Multiconfiguration Time-Dependent Hartree Method. The model for heterogeneous ET reactions at dye−semiconductor interfaces introduced above is a typical example for quantum dynamics of a complex molecular system embedded in a condensed phase environment. In addition to the relatively large number of intramolecular modes of the C343 chromophore, the model requires the dynamical description of two continua, the electronic states of the conduction band of the semiconductor and the mode continuum, which models the solvent environment. To simulate the quantum dynamics of this system, we use the multilayer (ML) formulation[43] of the multiconfiguration time-dependent Hartree (MCTDH) method[66−69] in combination with an importance sampling scheme to describe the thermal initial conditions in the observables introduced above. The method as well as applications to different reactions in the condensed phase have been described in detail previously.[40,43,70] Here, we only briefly introduce the general idea and give some details specific to the application in this work.

All observables introduced above can be written in the form of correlation functions

$$C_{AB}(t) = \mathrm{tr}[\rho_N A\, e^{iHt} B\, e^{-iHt}] \quad (29a)$$

Here, A and B denote operators describing physical observables of interest (e.g., the reduced electronic or vibrational density matrix, dipole moment, etc.). Operator A, furthermore, includes the initial state of the electronic degrees of freedom. ρ_N is the initial density matrix for the nuclear degrees of freedom

$$\rho_N = \frac{1}{Q_N} e^{-\beta H_{Ng}} \quad (29b)$$

and $Q_N = \mathrm{tr}[e^{-\beta H_{Ng}}]$ is the corresponding partition function. To evaluate the trace, we use a direct product basis $|n\rangle |\phi_j\rangle$, where the "nuclear" states $\{|n\rangle\}$ are the eigenstates of H_{Ng}, i.e.,

$$\rho_N = \sum_n p_n |n\rangle \langle n| \quad (30a)$$

Employing, furthermore, the representation

$$A = \sum_j \sum_i a_{ij} |\phi_i\rangle \langle\phi_j| \quad (30b)$$

where $a_{ij} \equiv \langle\phi_i| A |\phi_j\rangle$, the evaluation of the trace leads to the following expression for $C_{AB}(t)$

$$C_{AB}(t) = \sum_n p_n \sum_j \sum_i a_{ij} \langle n| \langle\phi_j| e^{iHt} B e^{-iHt} |\phi_i\rangle |n\rangle$$
$$= \sum_n p_n \sum_j \sum_i a_{ij} \langle\Psi^j_n(t)| B |\Psi^i_n(t)\rangle \quad (31)$$

where

$$|\Psi^i_n(t)\rangle = e^{-iHt} |\Psi^i_n(0)\rangle = e^{-iHt} |\phi_i\rangle |n\rangle \quad (32)$$

Thus, the major computational task is to solve the time-dependent Schrödinger equations

$$i \frac{\partial}{\partial t} |\Psi^i_n(t)\rangle = H |\Psi^i_n(t)\rangle \qquad n, i = 1, 2, ... \quad (33a)$$

with initial conditions

$$|\Psi^i_n(0)\rangle = |n\rangle |\phi_i\rangle \quad (33b)$$

which are selected according to the probability distribution p_n using an importance sampling scheme.

To solve the time-dependent Schrödinger equations (33a), we employ the multilayer (ML) formulation[43] of the multiconfiguration time-dependent Hartree method (MCTDH). To introduce the basic idea of this method, let us first briefly discuss the original (single-layer) MCTDH theory.[66−69] In this method, the overall wave function is expanded in terms of many time-dependent configurations

$$|\Psi(t)\rangle = \sum_J A_J(t) |\Phi_J(t)\rangle$$
$$= \sum_{j_1} \sum_{j_2} \cdots \sum_{j_M} A_{j_1 j_2 \cdots j_M}(t) \prod_{k=1}^{M} |\phi^k_{j_k}(t)\rangle \quad (34)$$

Here $|\phi^k_{j_k}(t)\rangle$ is the "single-particle" (SP) function for the k-th SP degree of freedom and M denotes the number of SP degrees of freedom. Each SP degree of freedom usually contains several (Cartesian) degrees of freedom in our calculation. The equations of motion (see, e.g., refs 43 and 66) for the configuration coefficients $A_J(t)$ and the SP functions $|\phi^k_{j_k}(t)\rangle$ are obtained by inserting the ansatz (eq 34) into the Dirac−Frenkel variational principle.[71]

In contrast to the time-independent configurations (corresponding to fixed $|\Phi_J\rangle$ in the expansion of eq 34) used in most of the conventional basis set approaches for wave packet propagation, the MCTDH method employs time-dependent configurations, which are variationally determined through the use of SP functions. This difference is the reason for the greater flexibility of the MCTDH wave function, which in turn makes the MCTDH method capable of handling many more degrees of freedom in a numerically exact way.[43,72−74]

If the number of degrees of freedom to be treated quantum mechanically becomes larger than ≈50−100, the original MCTDH method reaches its limits within the currently available computer technology. To simulate systems with even more degrees of freedom, it is more efficient to use the ML-MCTDH method.[43] In this approach, the SP functions $|\phi^k_n(t)\rangle$ in the original (single-layer) MCTDH method are further expressed employing a multiconfiguration expansion. For two layers, the expansion reads

$$|\phi^k_n(t)\rangle = \sum_I B^{k,n}_I(t) |u^k_I(t)\rangle$$
$$\equiv \sum_{i_1} \sum_{i_2} \cdots \sum_{i_{Q(k)}} B^{k,n}_{i_1 i_2 \cdots i_{Q(k)}}(t) \prod_{q=1}^{Q(k)} |v^{k,q}_{i_q}(t)\rangle \quad (35)$$

where $Q(k)$ denotes the number of level two (L2) SP degrees of freedom in the k-th level one (L1) SP and $|v^{k,q}_{iq}(t)\rangle$ is the L2 SP function. The expansion of the overall wave function can thus be written in the form

$$|\Psi(t)\rangle = \sum_{j_1} \sum_{j_2} \cdots \sum_{j_M} A_{j_1 j_2 \cdots j_M}(t) \times$$
$$\prod_{k=1}^{M} [\sum_{i_1} \sum_{i_2} \cdots \sum_{i_{Q(k)}} B^{k,j_k}_{i_1 i_2 \cdots i_{Q(k)}}(t) \prod_{q=1}^{Q(k)} |v^{k,q}_{i_q}(t)\rangle] \quad (36)$$

As in the original MCTDH theory, the equations of motion[43] for the configuration coefficients $A_J(t)$, $B^{k,n}_I(t)$, and the single particle functions of the first and second layer are obtained employing the Dirac−Frenkel variational principle.[71]

The ML-MCTDH method, as well as the original MCTDH method, are rigorous (in principle numerically exact) quantum dynamical methods; that is, if a sufficiently large number of SP functions are included, the solution of the equations of motion converges to the solution of the time-dependent Schrödinger equation. Including several dynamically optimized layers builds in more flexibility in the variational functional. As a result, the ML MCTDH approach has the capability of treating substantially more physical degrees of freedom than the original MCTDH approach.

Because in the dynamical method used all degrees of freedom are treated explicitly, the continuum of electronic states (describing the conduction band of the semiconductor) as well as the continuous distribution of solvent modes are first discretized and represented by a finite number of states and modes, respectively. Thereby, the actual number of modes (states) necessary to represent the true continuum depends on the specific parameters considered and the time scale of interest and serves as a convergence parameter. The details of efficiently discretizing the continuum of electronic states and the continuous distribution of vibrational modes have been given previously in refs 40 and 41, respectively, and will not be repeated here. For the system considered below, the number of bath modes required varies between 30 and 50 and the number of electronic states between 200 and 400 (depending on the time scale of interest).

III. Results and Discussion

In this section, we present results of simulations of electron injection dynamics and the associated nuclear motion for the dye−semiconductor system C343−TiO_2 based on the model introduced in section 2.A. We first consider the absorption spectra of the dye−semiconductor system. Figure 4 shows a comparison of experimental[11,64] and simulated absorption spectra for the chromophore C343 with (full lines) and without (dashed lines) adsorption to TiO_2 nanoparticles. In both spectra, the system was embedded in a solvent environment. As was discussed in section 2.A, the comparison of simulated and experimental absorption spectra has been used to determine four parameters of the ET model: the overall solvent reorganization energy with respect to the excitation of C343 ($\lambda^d_b = 1400$ cm^{-1}), the overall strength of the electronic coupling between chromophore and titanium oxide ($v_0 = 4000$ cm^{-1}), the energy

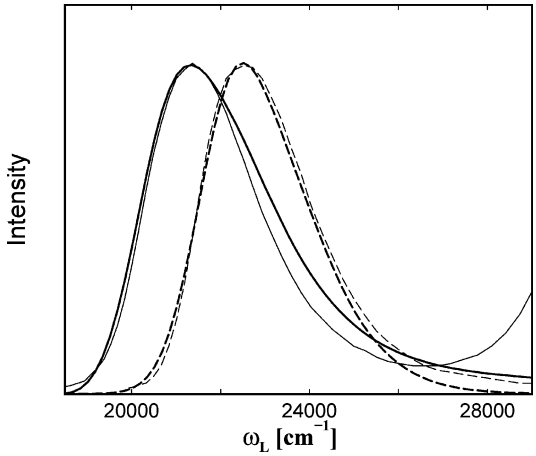

Figure 4. Absorption spectra of the chromophore C343 in solution with (full lines) and without (dashed lines) adsorption to titanium oxide nanoparticles. The simulated spectra (thick lines) are compared to experimental results (thin lines) from refs 11 and 64.

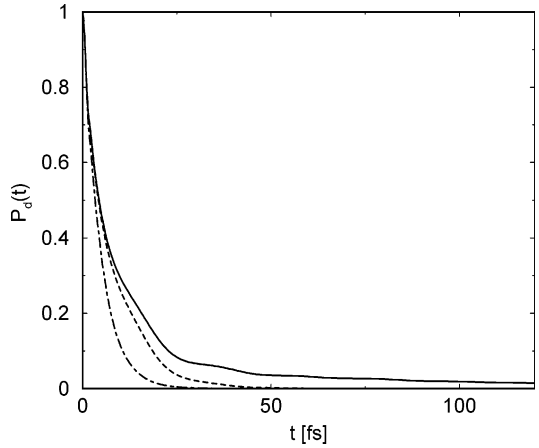

Figure 5. Electron injection dynamics of the C343−titanium oxide system. Shown is the population of the donor state after photoexcitation with (full line) and without (dashed−dotted line) coupling to the nuclear degrees of freedom. The dashed line depicts the results of a calculation where only the vibrational degrees of freedom of C343 have been taken into account and the coupling to the solvent environment has been neglected.

of the donor state relative to the lower conduction band edge of titanium oxide ($\epsilon_d = 4308$ cm^{-1}), and the energy of the ground state ($\epsilon_g = -18708$ cm^{-1}). These values correspond to a situation where the energy of the donor state is located well above the conduction band edge (the minimum of the energy of the donor state is $\epsilon_d - \sum_l \lambda_l^d - \lambda_b^d = 1990$ cm^{-1} [76]) and a relatively strong coupling between the chromophore and the semiconductor substrate. The potential energy surfaces of the ET model are schematically illustrated in Figure 1.

As Figure 4 demonstrates, the model with the thus determined parameters describes the low energy part of the two experimental absorption spectra quite well. The deviations between experimental and theoretical results in the higher energy part are related to contributions of a higher electronically excited state [in the case of the isolated chromophore (dashed lines)] and direct valence-conduction band excitation of titanium oxide [in the case of the absorption spectrum of the dye−semiconductor complex (full lines)]. Both effects are not included in the current model because in the energy range of interest they are expected to be of minor importance for the dynamics of the injection process.

Next, we consider the electron injection dynamics. The result of the simulation of the ET dynamics shown in Figure 5 exhibits an ultrafast injection of the electron from the electronically excited state of the C343 chromophore into the semiconductor: More than 80% of the population of the initially prepared donor state decays within 20 fs into the conduction band of titanium oxide. This time scale is at the lower boundary of experimental results for the C343−TiO_2 system, where injection times in the range of 20−200 fs have been found using different techniques.[3,5,11,18,19] In addition to the dominating ultrafast injection, the simulation results also show a small component with slower injection dynamics (see below).

To investigate the effect of the nuclear degrees of freedom on the electron injection dynamics, Figure 5 also depicts the result for the population dynamics of the donor state based on a purely electronic calculation (dashed−dotted line), where the coupling to all nuclear degrees of freedom has been neglected, as well as the result of a calculation where the coupling to the solvent environment has been neglected (dashed line). The comparison of the purely electronic and the full (vibronic) results shows that the coupling to the nuclear degrees of freedom has a significant effect on the ET dynamics. In particular, it results in an overall slower injection dynamics; that is, the electron is to some extent stabilized at the donor state. The comparison of the full calculation with the result where the coupling to the solvent environment has been neglected reveals that for short times the major effect is due to coupling to the intramolecular vibrations of C343. For longer times, the coupling to the solvent provides an additional stabilization mechanism for the electron. It is also seen that the coupling to the vibrational degrees of freedom of C343 results in small oscillatory structures superimposed on the decay of the population of the donor state. We have analyzed in detail the mutual influence of electronic and nuclear degrees of freedom in the dynamics of the C343−titanium oxide system. Because of the large number of vibrational modes of C343, here we can only discuss a few selected but representative examples.

Because of the ultrafast injection dynamics, only high-frequency intramolecular modes of C343 can have a significant impact on the ET dynamics. As an example for such a mode, Figure 6 (left side) shows the vibrational wave packet dynamics of a ν(C−C) + δ(CH) vibration ($\Omega = 1612$ cm^{-1}) in the donor and acceptor state, respectively. Because of the displacement of the excited and ground state minima along this coordinate ($\lambda^d = 230$ cm^{-1}), the photoexcitation process triggers wave packet motion along this mode in the donor state. This vibrational motion (in combination with other high-frequency vibrations) causes the oscillatory structure in the decay characteristics of the population of the donor state. It is also seen that the coherent vibrational motion "survives" the electron injection process and is therefore also present in the acceptor state.

While a direct dynamical influence of vibrational coherence on the ET process is only possible for high-frequency (fast) modes, low-frequency (slow) modes exhibit another interesting effect due to electronic vibrational coupling. As an example, Figure 6 (right side) shows wave packet motion of the low-frequency vibration of the nitrogen group ($\Omega = 133$ cm^{-1}). This mode has negligible changes in equilibrium geometry with respect to photoexcitation ($\lambda^d = 2$ cm^{-1}) but shows a rather large displacement with respect to the ET process, i.e., the transition from the photoexcited state to the cation ($\lambda^{ET} = 183$ cm^{-1}). As a result, the photoexcitation prepares an (with respect to this mode) essentially stationary wave packet in the donor state. On the other hand, the wave packet in the acceptor states

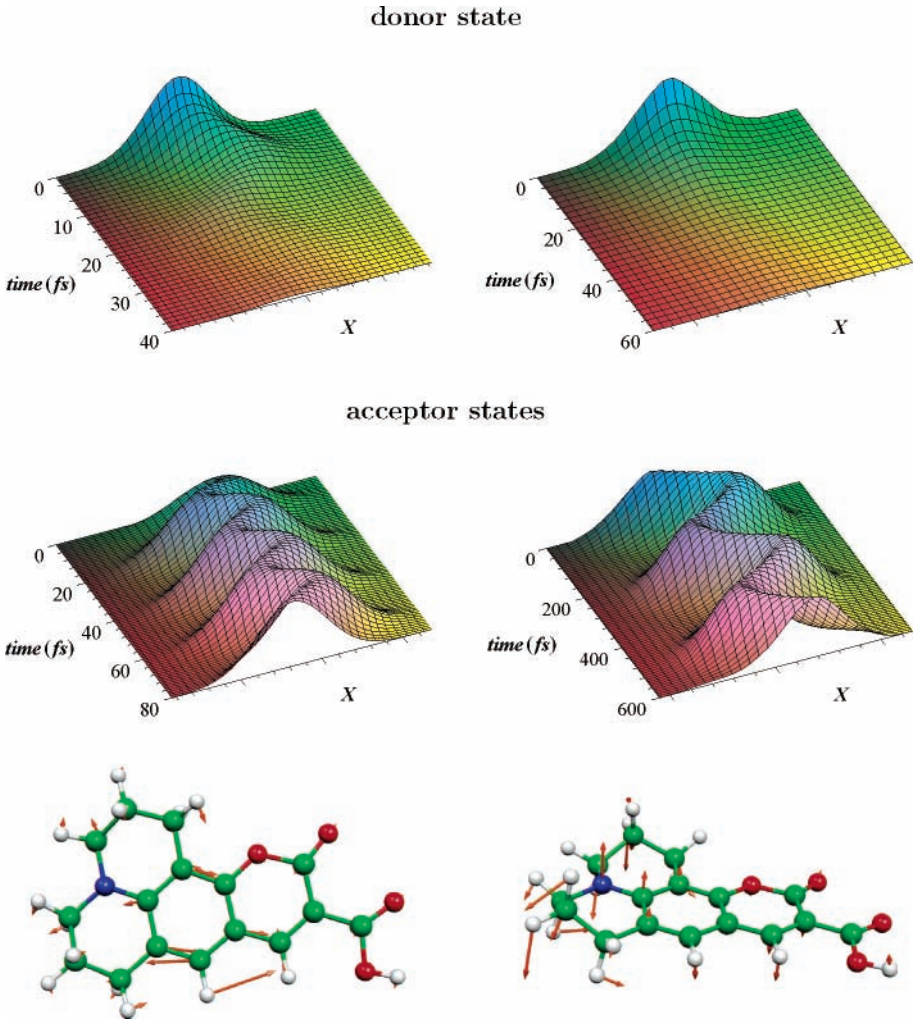

Figure 6. Wave packet dynamics of two representative vibrational normal modes of C343 after photoexcitation. Shown is the reduced density of a high-frequency ν(C−C) + δ(CH) vibration (Ω = 1612 cm^{-1}, left side) and the low-frequency vibration of the nitrogen group (Ω = 133 cm^{-1}, right side) in the donor state (upper panel) and averaged over the acceptor states (lower panel), respectively.

shows pronounced oscillatory motion. This motion is induced by the ET process, the time scale of which ($\approx$ 20 fs) is more than one order of magnitude faster than the vibrational period of the mode ($t = 2\pi/\Omega \approx 251$ fs). Thus, similar to ultrafast photoexcitation, the ultrafast ET process prepares a coherent wave packet on the potential energy surface of the acceptor states, which then (due to the relatively large reorganization energy) starts to oscillate.

The two examples discussed above demonstrate that within the same molecule—depending on the time scale of nuclear motion—electronic vibrational coupling can result in ET driven by coherent vibrational motion as well as vibrational motion induced by ET. Thus, the heterogeneous ET reaction in the C343−TiO_2 system is another example of a photoreaction, which cannot be described by rate theories, such as, for example, the traditional Marcus theory of ET,[77] because the fundamental assumption of a time scale separation between ET dynamics and nuclear motion is not fulfilled.

Because the results presented above are based on a model, where some parameters have been determined empirically by fitting experimental data, it is important to study the dependence of the results for the ET dynamics with respect to variations of the parameters. As an example, Figure 7 shows a comparison of results, which have been obtained for different values of the overall electronic coupling strength, υ_0, between C343 and TiO_2. Within this range of parameters, the simulated absorption spectra

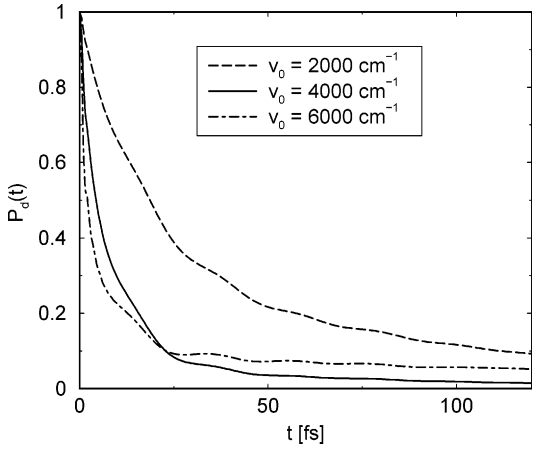

Figure 7. Electron injection dynamics of the C343−titanium oxide system. Shown is the population of the donor state after photoexcitation for three different values of the overall C343−TiO_2 coupling strength: υ_0 = 2000 cm^{-1} (dashed line), υ_0 = 4000 cm^{-1} (full line), and υ_0 = 6000 cm^{-1} (dashed−dotted line).

are still in reasonable agreement with the experimental results. It is seen that for short times the injection becomes faster for increasing coupling. It is noted, however, that the injection rate at short times does not follow a simple rate behavior ($\sim\upsilon_0^2$) but increases slower with the coupling strength υ_0. Furthermore,

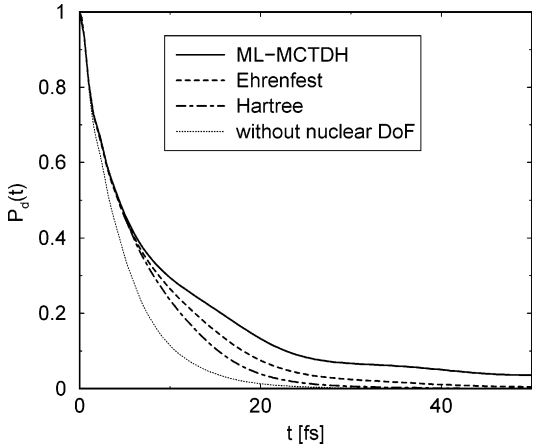

Figure 8. Electron injection dynamics of the C343−titanium oxide system. Shown is the population of the donor state after photoexcitation as obtained by the ML-MCTDH method (full line) and various approximate approaches: the classical Ehrenfest model (dashed line), the time-dependent Hartree method (dashed−dotted line), and the result that neglects the coupling to nuclear degrees of freedom (thin dotted line). The latter (purely electronic) result can be easily obtained from any conventional quantum mechanical approach.

for stronger coupling, the injection characteristics develop an additional slowly decaying component, the time scale of which increases with coupling strength. As has been discussed previously,[40] the appearance of such long-lived states is related to the proximity of the donor state to the conduction band edge. Although the energy of the donor state at the Franck−Condon geometry is well above the lower edge of the conduction band—and thus the purely electronic injection dynamics exhibits a fast and monotonic decay of the population of the donor state (see, e.g., the dashed−dotted line in Figure 5)—energy dissipation into the nuclear degrees of freedom results in an effectively lower electronic energy closer to the conduction band edge. Furthermore, during the dynamics, the nuclear wave packet may enter regions of configuration space that have a smaller effective coupling to the acceptor states due to smaller Franck−Condon overlap factors. Both mechanisms may cause a slower injection of the electron. Similar results are obtained (data not shown) if the location energy of the donor state ϵ_d relative to the conduction band edge is varied. We thus conclude that within the range of parameters, which provides a reasonable agreement of the experimental and the simulated absorption spectrum, the results for the injection dynamics do not change qualitatively.

The results presented above have been obtained employing the ML-MCTDH method, which allows an accurate treatment of the quantum dynamics. It can therefore also be used to study the capability of approximate methods to describe ET dynamics. As an example, Figure 8 shows a comparison with calculations based on the time-dependent self-consistent field method (sometimes also called time-dependent Hartree method)[78,79] and the Ehrenfest model.[80−87] While in the former method the wave function is assumed to be of product form, i.e., all correlations between different nuclear degrees of freedom are neglected, in the latter approach, all nuclear degrees of freedom are treated classically. The results in Figure 8 show that both approximations capture the short time dynamics reasonably well. For longer times, however, they predict a too fast electron injection process; that is, both methods underestimate the stabilization effect of the nuclear degrees of freedom on the electron. Thereby, as found previously for other systems,[88] the Ehrenfest model is in better agreement with the accurate quantum result than the mean field method. As has been discussed in ref 88, this is due to the fact that the Ehrenfest model (even for temperature $T = 0$ K) involves sampling over many trajectories (determined by the phase space distribution of the initial state), which captures some of the correlation effects.

IV. Conclusions

In this paper, we have studied the dynamics of photoinduced heterogeneous ET processes at dye−semiconductor interfaces. As an example, we have considered coumarin 343 adsorbed at a TiO_2 substrate. To describe the ET dynamics in this system, we have used a semiempirical model based on an Anderson−Newns type Hamiltonian and a simple tight-binding parametrization of the semiconductor substrate. The vibrational degrees of freedom of C343 as well as the electronic vibrational coupling parameters were characterized by electronic structure calculations. The influence of the surrounding solvent was taken into account based on a linear response model. To describe the dynamics of the model, the ML-MCTDH method was employed, which allows an accurate treatment of the quantum dynamics of large systems. Furthermore, we have studied the capability of two approximate dynamical methods, the time-dependent Hartree method and the Ehrenfest model, to describe the electron injection dynamics in the C343−TiO_2 system.

The simulation of the ET dynamics predicts an ultrafast, nonexponential injection process from the photoexcited donor state into the conduction band of TiO_2 on a time scale of $\approx$20 fs. This time scale is in the range of injection times found experimentally.[3,5,11,18,19] Despite the ultrafast time scale of the electron injection process, the results show a significant influence of the coupling to the nuclear degrees of freedom. In particular, the coupling to the nuclear degrees of freedom results in an overall slower injection dynamics. A detailed analysis of the vibrational motion of the intramolecular modes of C343 revealed that the specific effect of the coupling to the vibrational degrees of freedom depends on the relative time scale of electronic and vibrational motion: The coupling to high-frequency modes of C343 can influence the ET process directly, resulting in oscillatory structures superimposed on the decay of the donor state, i.e., vibrational coherence. For low-frequency modes, on the other hand, we have found that the ultrafast ET can induce vibrational motion, a process that cannot be described within the traditional Marcus theory of ET.

In the present study, we have assumed a preparation of the initial (donor) state by a laser pulse that is short as compared to all time scales of the ET system. The ML-MCTDH method can also be used to study the effect of a finite laser pulse on the dynamics of the ET reaction. For this purpose, the coupling to the laser field has to be included in the simulation.[89] This will also allow an accurate simulation of time-resolved, e.g., pump−probe spectra and thus a direct comparison with experimental results.

Acknowledgment. I.K. and M.T. thank Wolfgang Domcke, Andreas Dreuw, Martin Lenz, and Josef Wachtveitl for helpful discussions. The generous allocation of computing time by the National Energy Research Scientific Computing Center (NERSC) and the Leibniz Rechenzentrum, Munich, is gratefully acknowledged. This work has been supported by the Deutsche Forschungsgemeinschaft and a collaborative research grant of the National Science Foundation (NSF) and the German Academic Exchange Service (DAAD). H.W. also acknowledges the NSF-CAREER award CHE-0348956 and the donors of the American Chemical Society Petroleum Research Fund for partial support of this research.

References and Notes

(1) Moser, J. E.; Grätzel, M. *Chem. Phys.* **1993**, *176*, 493.
(2) Hagfeldt, A.; Grätzel, M. *Chem. Rev.* **1995**, *95*, 49.
(3) Rehm, J. M.; McLendon, G. L.; Nagasawa, Y.; Yoshihara, K.; Moser, J.; Grätzel, M. *J. Phys. Chem.* **1996**, *100*, 9577.
(4) Martini, I.; Odak, J.; Hartland, G. V.; Kamat, P. V. *J. Chem. Phys.* **1997**, *107*, 8064.
(5) Wachtveitl, J.; Huber, R.; Spörlein, S.; Moser, J.; Grätzel, M. *Int. J. Photoenergy* **1999**, *1*, 131.
(6) Zimmermann, C.; Willig, F.; Ramakrishna, S.; Burfeindt, B.; Pettinger, B. *J. Phys. Chem. B* **2001**, *105*, 9245.
(7) Asbury, J.; Hao, E.; Wang, Y.; Ghosh, H. N.; Lian, T. *J. Phys. Chem. B* **2001**, *105*, 4545.
(8) Ramakrishna, G.; Gosh, H. N. *J. Phys. Chem. A* **2002**, *106*, 2545.
(9) Schnadt, J.; Brühwiler, P. A.; Patthey, L.; O'Shea, J. N.; Södergreen, S.; Odellus, M.; Ahuja, R.; Karis, O.; Bässler, M.; Persson, P.; Siegbahn, H.; Lunell, S.; Martenson, N. *Nature* **2002**, *418*, 620.
(10) Walters, K. A.; Gaal, D. A.; Hupp, J. T. *J. Phys. Chem. B* **2002**, *106*, 5139.
(11) Huber, R.; Moser, J. E.; Grätzel, M.; Wachtveitl, J. *Chem. Phys. Lett.* **2002**, *285*, 39.
(12) Huber, R.; Moser, J. E.; Grätzel, M.; Wachtveitl, J. *J. Phys. Chem. B* **2002**, *106*, 6494.
(13) Kallioinen, J.; Benkö, G.; Sundström, V.; Korrpi-Tommola, J.; Yartsev, A. *J. Phys. Chem. B* **2002**, *106*, 4396.
(14) Takeshita, K.; Sasaki, Y.; Kobashi, M.; Tanaka, Y.; Maeda, S.; Yamakata, A.; Ishibashi, T.; Onishi, H. *J. Phys. Chem. B* **2003**, *107*, 4156.
(15) Wang, L.; Ernstorfer, R.; Willig, F.; May, V. *J. Phys. Chem. B* **2005**, *109*, 9589.
(16) Hagfeldt, A.; Grätzel, M. *Acc. Chem. Res.* **2000**, *33*, 269.
(17) Grätzel, M. *Nature* **2001**, *414*, 338.
(18) Murakoshi, K.; Yanagida, S.; Capel, M.; Castner, E. In *Nanostructured Materials: Clusters, Composites, and Thin Films*; Shalaev, V. M., Moskovits, M., Eds.; American Chemical Society: Washington, DC, 1997.
(19) Gosh, H. N.; Asbury, J. B.; Wang, Y.; Lian, T. *J. Phys. Chem. B* **1998**, *102*, 10208.
(20) Willig, F.; Zimmermann, C.; Ramakrishna, S.; Storck, W. *Electrochim. Acta* **2000**, *45*, 4565.
(21) Benkö, G.; Kallioinen, J.; Korppi-Tommola, J.; Yartsev, A.; Sundström, V. *J. Am. Chem. Soc.* **2002**, *124*, 489.
(22) Huber, R.; Spörlein, S.; Moser, J.; Grätzel, M.; Wachtveitl, J. *J. Phys. Chem. B* **2002**, *104*, 8995.
(23) Hao, E.; Anderson, N.; Asbury, J.; Lian, T. *J. Phys. Chem. B* **2002**, *106*, 10191.
(24) Asbury, J.; Hao, E.; Wang, Y.; Lian, T. *J. Phys. Chem. B* **2000**, *104*, 11957.
(25) Rego, L.; Batista, V. *J. Am. Chem. Soc.* **2003**, *125*, 7989.
(26) Stier, W.; Prezhdo, O. *Isr. J. Chem.* **2002**, *42*, 213.
(27) Stier, W.; Prezhdo, O. *J. Phys. Chem. B* **2002**, *106*, 8047.
(28) Stier, W.; Prezhdo, O. *Adv. Mater.* **2004**, *16*, 240.
(29) Duncan, W.; Stier, W.; Prezhdo, O. *J. Am. Chem. Soc.* **2005**, *127*, 7941.
(30) Duncan, W.; Stier, W.; Prezhdo, O. *J. Phys. Chem. B* **2005**, *109*, 365.
(31) Rego, L.; Batista, V. *J. Chem. Phys.* **2005**, *122*, 154709.
(32) Newns, D. *Phys. Rev.* **1969**, *178*, 1123.
(33) Ramakrishna, S.; Willig, F.; May, V. *Phys. Rev. B* **2000**, *62*, 16330.
(34) Ramakrishna, S.; Willig, F. *J. Phys. Chem. B* **2000**, *104*, 68.
(35) Ramakrishna, S.; Willig, F.; May, V. *J. Chem. Phys.* **2001**, *115*, 2743.
(36) Schreiber, M.; Kondov, I.; Kleinekathöfer, U. *J. Lumin.* **2001**, *94*, 471.
(37) Ramakrishna, S.; Willig, F.; May, V. *Chem. Phys. Lett.* **2002**, *351*, 242.
(38) Ramakrishna, S.; Willig, F.; May, V. *J. Phys. Chem. B* **2003**, *107*, 607.
(39) Wang, L.; May, V. *J. Chem. Phys.* **2004**, *121*, 8039.
(40) Thoss, M.; Kondov, I.; Wang, H. *Chem. Phys.* **2004**, *304*, 169.
(41) Wang, H.; Thoss, M.; Miller, W. H. *J. Chem. Phys.* **2001**, *115*, 2979.
(42) Wang, H.; Thoss, M. *Isr. J. Chem.* **2002**, *42*, 167.
(43) Wang, H.; Thoss, M. *J. Chem. Phys.* **2003**, *119*, 1289.
(44) Kondov, I.; Thoss, M.; Wang, H. *Int. J. Quantum Chem.* In press.
(45) Hara, K.; Sayama, K.; Ohga, Y.; Shinpo, A.; Suga, S.; Arakawa, H. *Chem. Commun.* **2001**, *6*, 569.
(46) Muscat, J.; Newns, D. *Progress in Surface Science*; Davison, S. G., Ed.; Pergamon: Oxford, 1978; Vol. 9.
(47) Sebastian, K. *J. Chem. Phys.* **1989**, *90*, 5056.
(48) Boroda, Y.; Voth, G. A. *J. Chem. Phys.* **1996**, *104*, 6168.
(49) Dushinski, F.; Sassetti, M.; Weiss, U. *Acta Physicochim. URSS* **1937**, *7*, 551.
(50) Ahlrichs, R.; Bär, M.; Häser, M.; Horn, H.; Kölmel, C. *Chem. Phys. Lett.* **1989**, *162*, 165.
(51) Kondov, I.; Wang, H.; Thoss, M. To be published.
(52) Petersson, A.; Ratner, M.; Karlsson, H. *J. Phys. Chem. B* **2000**, *104*, 8498.
(53) Weiss, U. *Quantum Dissipative Systems*, 2nd ed.; World Scientific: Singapore, 1999.
(54) Makri, N. *J. Phys. Chem. B* **1999**, *103*, 2823.
(55) Georgievskii, Y.; Hsu, C.-P.; Marcus, R. A. *J. Chem. Phys.* **1999**, *110*, 5307.
(56) Rips, I.; Jortner, J. *J. Chem. Phys.* **1987**, *87*, 2090.
(57) May, V.; Kühn, O. *Charge and Energy Transfer Dynamics in Molecular Systems*; Wiley-VCH: Berlin, 2000.
(58) Cho, M.; Fleming, G. *Adv. Chem. Phys.* **1999**, *107*, 311.
(59) It is noted that in principle there are two possible solutions $\lambda_b^a = (\sqrt{\lambda_b^d} \pm \sqrt{\lambda_b^{ET}})^2$; however, for the set of parameters studied in this paper, the second solution would result in a rather large reorganization energy λ_b^{ga} and has therefore been excluded.
(60) Schulten, K.; Tesch, M. *Chem. Phys.* **1991**, *158*, 421.
(61) Bader, J.; Chandler, D. *J. Chem. Phys.* **1992**, *99*, 4391.
(62) Jimenez, R.; Fleming, G. R.; Kumar, P. V.; Maroncelli, M. *Nature* **1994**, *369*, 471.
(63) Stratt, R. M.; Maroncelli, M. *J. Phys. Chem.* **1996**, *100*, 12981.
(64) Huber, R. Ph.D. Thesis, Ludwig Maximilians University Munich, unpublished, 2002.
(65) Wang, H.; Thoss, M. To be published.
(66) Meyer, H.-D.; Manthe, U.; Cederbaum, L. S. *Chem. Phys. Lett.* **1990**, *165*, 73.
(67) Manthe, U.; Meyer, H.-D.; Cederbaum, L. S. *J. Chem. Phys.* **1992**, *97*, 3199.
(68) Beck, M. H.; Jäckle, A.; Worth, G. A.; Meyer, H.-D. *Phys. Rep.* **2000**, *324*, 1.
(69) Meyer, H.-D.; Worth, G. A. *Theor. Chem. Acc.* **2003**, *109*, 251.
(70) Thoss, M.; Wang, H. *Chem. Phys.* In press.
(71) Frenkel, J. *Wave Mechanics*; Clarendon Press: Oxford, 1934.
(72) Raab, A.; Worth, G.; Meyer, H.-D.; Cederbaum, L. *J. Chem. Phys.* **1999**, *110*, 936.
(73) Wang, H. *J. Chem. Phys.* **2000**, *113*, 9948.
(74) Huarte-Larranaga, F.; Manthe, U. *J. Phys. Chem. A* **2001**, *105*, 2522.
(75) Wang, H.; Thoss, M. *J. Phys. Chem. A* **2003**, *107*, 2126.
(76) It is noted that the value of $\epsilon_d - \sum_l \lambda_l^d - \lambda_b^d = 1990\ cm^{-1}$ for the minimum of the donor state has been calculated taking into account the 38 modes explicitly included in the dynamical calculation (i.e., $\lambda_s^d = 918\ cm^{-1}$). Including all modes of C343 (corresponding to $\lambda_s^d = 1010\ cm^{-1}$) would result in the slightly lower value of $1898\ cm^{-1}$.
(77) Marcus, R. A.; Sutin, N. *Biochim. Biophys. Acta* **1985**, *811*, 265.
(78) Gerber, R. B.; Buch, V.; Ratner, M. A. *J. Chem. Phys.* **1982**, *77*, 3022.
(79) Stock, G. *J. Chem. Phys.* **1995**, *103*, 1561.
(80) Tully, J. C.; Preston, R. K. *J. Chem. Phys.* **1971**, *55*, 562.
(81) Mott, N. F. *Proc. Cambridge Philos. Soc.* **1931**, *27*, 553.
(82) Delos, J. B.; Thorson, W. R.; Knudson, S. K. *Phys. Rev. A* **1972**, *6*, 709.
(83) Billing, G. D. *Chem. Phys. Lett.* **1975**, *30*, 391.
(84) Micha, D. A. *J. Chem. Phys.* **1983**, *78*, 7138.
(85) Graham, R.; Höhnerbach, M. *Z. Phys. B* **1984**, *57*, 233.
(86) Billing, G. D. *J. Chem. Phys.* **1993**, *99*, 5849.
(87) Stock, G. *J. Chem. Phys.* **1995**, *103*, 2888.
(88) Stock, G.; Thoss, M. *Adv. Chem. Phys.* **2005**, *131*, 243.
(89) Wang, H.; Thoss, M. *Chem. Phys. Lett.* **2004**, *389*, 43.